

Cover sheet for:

The influence of orbital parameters on the North American Monsoon system during the Last Interglacial Period

Nadja Insel

Northeastern Illinois University, Department of Earth Science
University of Chicago, Department of Geophysical Sciences

Max Berkelhammer

University of Illinois at Chicago, Department of Earth and Environmental Sciences

This manuscript has been submitted for publication in *Journal of Quaternary Studies*. Please note that the paper has undergone one round of reviews and has been revised but not accepted. Subsequent versions of the manuscript will therefore have slightly different content. Upon acceptance, the final version of this manuscript will be available via "Peer-reviewed Publication DOI" link from EarthArXiv. Please feel free to contact the authors for any matters relating to this manuscript.

1 1 **The influence of orbital parameters on the North American Monsoon system during the** 2 3 4 5 2 **Last Interglacial Period**

6
7 3
8 4 Nadja Insel^{1,3}, Max Berkelhammer²

9 5 ¹Northeastern Illinois University, Department of Earth Science

10 6 ²University of Illinois at Chicago, Department of Earth and Environmental Sciences

11 7 ³Research Associate, University of Chicago, Department of Geophysical Sciences

12 13 14 9 15 16 10 **Abstract**

17 11 The response of summer precipitation in the western U.S. to climate variability remains a subject
18 12 of uncertainty. For example, paleoclimate records indicate the North American monsoon (NAM)
19 13 was stronger and spatially more extensive during the Holocene, whereas recent modeling suggests
20 14 a weakened NAM response to increasing temperatures. These illustrate diverging pictures of the
21 15 NAM response to warming. Here, we examine summer precipitation in the southwestern U.S.
22 16 related to Last Interglacial insolation forcing. Using a high-resolution climate model, we find that
23 17 Eemian insolation forcing results in overall wetter conditions throughout most of the southwestern
24 18 U.S, but significantly drier than present conditions over Arizona. The overall wetter conditions are
25 19 associated with a northward shift of the anticyclonic circulation aloft and increased moisture in the
26 20 lower and mid-troposphere during the Eemian. Increased advection of Gulf of Mexico moisture is
27 21 responsible for increasing precipitation in New Mexico and the northern edges of the NAM region.
28 22 Drier conditions over Arizona are likely related to reduced local convection and enhanced
29 23 north/northwest passage of tropical cyclone remnants. These results highlight the spatial
30 24 complexity of the NAM response to increasing radiative forcing and allow a better understanding
31 25 of monsoon dynamics and variability in response to a warming climate.

32 33 34 26 35 27 **1. Introduction**

36 28 Precipitation in the southwestern United States is dominated by seasonal monsoonal circulation.
37 29 The North American Monsoon (NAM) occurs mainly between July and September and provides
38 30 ~70% of mean annual precipitation to central and northern Mexico and ~35-50% of mean annual
39 31 precipitation to Arizona and New Mexico in the U.S. (Fig. 1a). The NAM shows a strong variability
40 32 on annual, decadal, and millennial timescales (e.g., Diem et al., 2013; Griffin et al., 2013; Poore et
41 33 al., 2005) and understanding the response of the monsoonal system to climate change is critical in
42 34 determining changes in the amount and seasonal distribution of precipitation in this semiarid region
43 35 of North America. The response of the NAM to increased greenhouse gas forcing and increasing

1
2
3 36 temperature is ambiguous. Previous studies have concluded that global warming was simply
4 37 delaying the North American monsoon, but changes in total monsoon seasonal rainfall are small
5 38 and insignificant (Cook and Seager, 2013). In contrast, a recent study by Pascale et al. (2017)
6 39 highlights the possibility of a strong precipitation reduction in the northern edge of the monsoon in
7 40 response to warming, with consequences for regional water resources, agriculture and ecosystems.
8 41 These suggested responses of the NAM to current changes in the climate system are distinct from
9 42 studies providing causes and characteristics of climatic and monsoonal variations over paleo
10 43 timescales. Insolation is widely regarded as an important control of climate change on long-
11 44 timescales, particularly in monsoon regions. A strong correlation between summer monsoon
12 45 intensity and summer insolation has been observed in monsoon records from Asia, South America,
13 46 and Africa (Cruz et al., 2005; Kutzbach and Liu, 1997; Liu et al., 2006; Wang et al., 2001).
14 47 Evidence suggests that during insolation maxima, increased summer land-sea temperature contrasts
15 48 strengthen monsoon systems and shift the summer position of the Intertropical Convergence Zone
16 49 (ITCZ) further inland (McKay et al., 2011; Montoya et al., 2000). Several records from the U.S.
17 50 and Mexico exhibit evidence of increased summer convection and precipitation during the warmest
18 51 periods of the mid-Holocene (Barron et al., 2012; Metcalfe et al., 2015).

19 52 To better understand the interplay between rising temperatures and moisture in the NAM region,
20 53 we chose to focus on the response of the NAM to shifts in orbital forcings during the Last
21 54 Interglacial (LIG: ~130 to 116ka). The LIG is the most recent period in Earth history when
22 55 temperatures are believed to have exceeded those of today (Bakker et al., 2013; CAPE members -
23 56 Anderson, 2006; Kukla et al., 2002; McKay et al., 2011; Turney and Jones, 2010). In particular,
24 57 the Eemian (~125 ka) is an interval where the Earth was in an orbital configuration that corresponds
25 58 with insolation maxima and enhanced summer heating of the Northern hemisphere (Berger and
26 59 Loutr, 1991). The Eemian was warmer than the present day with higher sea level (Bard et al., 1990)
27 60 and diminished ice sheets (Cuffey and Marshall, 2000). Climate models suggest that the Eemian
28 61 was a time of increased Northern-Hemisphere temperature and humidity, with a northward-shifted
29 62 ITCZ, increased summer land-sea temperature contrast, and intensified monsoon convection
30 63 (Montoya et al., 2000). Numerous studies have focused on the response of polar temperatures to
31 64 interglacial forcing but less attention has been paid to the regional hydroclimatic changes at the
32 65 time. These changes are of interest because the response of terrestrial ecosystems to hydroclimate
33 66 shifts may have been critical to the carbon cycle during the Eemian (Kleinen et al., 2016). For
34 67 example, favorable redistributions of rainfall into semi-arid regions such as the Southwestern U.S.
35 68 may have acted to increase the terrestrial carbon sink.

36
37
38
39
40
41
42
43
44
45
46
47
48
49
50
51
52
53
54
55
56
57
58
59
60

1
2
3 69 Here, we use simulations from a regional climate model (RegCM) under LIG and modern forcings
4 70 to evaluate changes in the strength, timing, duration, and amount of moisture transported from
5 71 different sources during the NAM season. The simulated periods are linked with different phases
6 72 of the interglacial climate system that have been identified in paleodata, namely: the maximum and
7 73 minimum summer insolation in the northern hemisphere (130 ka and 115ka, respectively) as well
8 74 as the minimum global ice volume (125 ka). Our simulations intend to complement previous LIG
9 75 simulations done at lower resolution with a focus on monsoonal dynamics. Among other things,
10 76 these simulations serve as a reference for new and upcoming proxy records in the southwestern
11 77 U.S. (Pigati et al., 2014). Particularly, the data provide background to consider how global carbon
12 78 cycle dynamics and ecological systems in the southwestern U.S. might have responded to recent
13 79 periods in Earth history when summer temperatures exceeded those of today (Brown et al., 2014;
14 80 Elias, 2014; Strickland et al., 2014) Understanding these variations is critical to forecast seasonal
15 81 supply of water to and habitat changes in the southwestern U.S. under current warming conditions.
16
17
18
19
20
21
22
23
24
25
26

27 84 **2. Model Description and Setup**

28 85 RegCM_4.4.5 (Pal et al., 2007) is a fourth generation, three-dimensional regional climate model,
29 86 based on the original model developed by Giorgi et al. (1993a; 1993b) with a dynamical core that
30 87 is adopted from the hydrostatic version of the Pennsylvania State University-National Center for
31 88 Atmospheric Research Mesoscale Model (MM5) (Grell et al., 1994). It is a primitive-equation,
32 89 hydrostatic, compressible model with sigma-vertical coordinates (Giorgi et al., 1993a).
33 90 Improvements in the software code and model physics (e.g., representation of convective schemes,
34 91 surface physics, atmospheric chemistry and aerosols, ocean-air exchanges) allows an enhanced
35 92 model performance in monsoonal regions. A full description of RegCM4's basic features and
36 93 details on the historical evolution of RegCM are given in Giorgi et al. (2012).

37 94 RegCM_4.4.5 experiments were performed for North America using a horizontal resolution of 55
38 95 km and 18 vertical levels. Lateral boundary conditions are based on data from ERA-Interim
39 96 reanalysis with a spatial resolution of 1.5°x1.5° (EIN15), while sea-surface temperatures (SSTs)
40 97 were obtained from the NOAA optimum interpolation (OI) SST analysis (Reynolds et al., 2002).
41 98 Convective precipitation was computed with the MIT-Emanuel scheme (Emanuel, 1991). It has
42 99 been shown that RegCM simulations with the cumulus convections scheme and its Emanuel closure
43 100 assumptions lead to improved simulations of precipitation, temperature and low-level wind patterns
44 101 in comparison to other cloud and convection parameterizations (Pal et al., 2007; Sinha et al., 2019;
45 102 Velikou and Tolika, 2017). In particular, RegCM has been widely applied in limited-domain,
46
47
48
49
50
51
52
53
54
55
56
57
58
59
60

1
2
3 103 seasonal forecasts and used to simulate climate in high-precipitation monsoonal regions and around
4 the globe (e.g., Diro et al., 2012; Fuentes-Franco et al., 2014; Insel et al., 2009; Sylla et al., 2010).
5 104
6 105 The goal of this study is to quantify the impact of orbital parameters on North American Monsoon
7
8 106 dynamics. Our model domain ranges from 128° W to 82° W along the southern domain margin at
9
10 107 ~10° N and from 150° W to 60° W along the northern domain margin at ~60° N (Fig. 1). The
11
12 108 domain includes parts of the western Pacific and the Gulf of Mexico to accurately simulate climate
13
14 109 sensitivity over oceanic regions. We designed 4 experiments to account for different orbital
15
16 110 parameter configurations during the LIG and changing greenhouse gas concentrations (Table 1). In
17
18 111 particular, we simulated interglacial time slices to capture the obliquity minimum and maximum
19
20 112 (MinObliquity-115ka, MaxObliquity-130ka; (Berger and Loutr, 1991)), respectively, and a third
21
22 113 time slice that falls between these two. Simulations were 21 years in length and results are based
23
24 114 on the last 10 years of the simulations. While the length of spin-up time is dependent on model
25
26 115 domain, season, and circulation intensity, previous studies have shown that regional climate models
27
28 116 are usually representing a dynamic equilibrium after just a few months (Zhong et al., 2007)

29
30 117 Small discrepancies with observations may arise due to the experimental design, which include
31
32 118 the use of present-day vegetation and polar ice sheets as well as consistent sea surface temperatures.
33
34 119 Modern boundary conditions for geography, ice sheets, and vegetation follow previous studies
35
36 120 simulating temperature and precipitation responses in the United States to interglacial warm periods
37
38 121 (e.g., Diffenbaugh et al., 2006; Otto-Bliesner et al., 2013). Moreover, Diffenbaugh et al. (2006)
39
40 122 indicated that general precipitation patterns over the U.S. do not change in response to sea surface
41
42 123 temperatures changes in orbital-driven warm periods. Moreover, they observed that at least some
43
44 124 localities showed greater agreement with the proxy record in experiments without changes in SSTs
45
46 125 as compared to a more complete ocean treatment.

47
48 126

49 127 **3. Results**

50 128 **3.1. Model Validation**

51 129 A comparison between simulated and observed data indicates that RegCM_4.4.5 performs well in
52
53 130 capturing the general climatology in the western part of North America (Fig. 1). The model
54
55 131 performance for modern precipitation is assessed by using independent precipitation observations
56
57 132 from the Global Precipitation Climatology Centre (GPCC) data base (Schneider et al., 2011).
58
59 133 Figure 1a shows the NAM expressed as percent of annual precipitation that falls in July to
60
61 134 September (JAS). The model captures the spatial distribution of monsoon precipitation across the
62
63 135 western United States and Mexico, including regions of maximum precipitation along the west
64
65 136 coast of Mexico (Fig 1b). Moreover, the model is consistent with the climatological monthly

1
2
3 137 precipitation averaged over the main region of the NAM. The region is semiarid with a single
4 138 precipitation maximum evident in the summer months with averaged maximum precipitation of
5 139 around 3.5 mm/day (Fig 1c). The model captures the July and August precipitation, but
6 140 overestimates precipitation in June and September. We attribute this discrepancy to the model
7 141 resolution and prescribed sea surface temperatures that likely overestimate the moisture component
8 142 that is transported from the oceans to the land, resulting in higher precipitation rates. A model data
9 143 comparison indicates a wet bias over the core of the NAM region in southern Mexico, and a dry
10 144 bias along the western continental Mexican coast. However, the main spatial and temporal patterns
11 145 of monsoonal precipitation are well established in our model simulations.
12
13
14
15
16
17
18

19 147 **3.2. Insolation and Temperature**

20 148 The changes in the amount of insolation received by the Earth during LIG result from changes in
21 149 the astronomical configuration. During MaxObliquity (130ka) and in the Eemian (125ka), our study
22 150 area received more insolation in spring and summer compared to the present-day period (Fig. 2a,
23 151 b). Focusing on the NAM area, the difference in incoming shortwave flux at the top of the
24 152 atmosphere between the warm LIG periods and present is approximately 45 Wm^{-2} in June and -25
25 153 Wm^{-2} in December. However, MaxObliquity indicates stronger insolation in particular from late
26 154 February to July, while the Eemian is characterized by stronger insolation from late April to
27 155 September (Fig. 2a). In contrast, MinObliquity (115 ka) indicates the opposite pattern in insolation
28 156 with below modern values in spring and summer and above modern values during the fall and
29 157 winter. The magnitude of changes between MinObliquity and modern is overall smaller with
30 158 around -20 Wm^{-2} in June and 20 Wm^{-2} in December.
31
32
33
34
35
36
37

38 159 In response to increased insolation in northern hemisphere spring and summer during 130ka and
39 160 125 ka, simulated surface temperatures are generally higher during those periods compared to the
40 161 present-day over the majority of the western and southwestern U.S. Positive temperature anomalies
41 162 averaged over the NAM region are observed in April, May and June during the early LIG (Fig. 2c,
42 163 d). Temperature anomalies indicate strong spatial variability with up to 2°C higher temperatures in
43 164 New Mexico and Arizona, but similar to present temperatures in central and western Mexico (Fig.
44 165 3). Warming is stronger and occurs earlier at 130ka in comparison to 125ka. In July and August,
45 166 surface temperatures are cooler in most parts of the monsoon region with regional temperature
46 167 differences of up to -1.5°C compared to present. Most cooling is observed along the west coast of
47 168 Mexico and Baja California. This is opposite to the expected direct radiative effect, and might be
48 169 due to increased cloudiness, evapotranspiration, and precipitation (Fig. 2e-f, 4). During
49
50
51
52
53
54
55
56
57
58
59
60

1
2
3 170 MinObliquity, surface temperatures in the southwestern U.S. are generally colder than present
4 171 throughout the entire spring and summer, corresponding to reduced insolation at that time (Fig. 3).

5
6 172

7 173 **3.3. North American Monsoon Pattern (Modern versus Eemian)**

8 174 Simulated precipitation is the sum of large-scale precipitation related to cyclones or frontal systems,
9 175 and convective precipitation associated with local surface heating and vertical air movement. The
10 176 NAM system is associated with a dramatic increase in summer precipitation. Averaged over the
11 177 entire monsoon region, precipitation magnitudes over land reach a maximum around 130
12 178 mm/month in July and August (Fig. 2e). Modern precipitation is spatially very variable with the
13 179 highest precipitation rates in Mexico and significant less precipitation across the southwestern U.S.
14 180 (Fig. 5a). Precipitation related to the NAM system comes from two distinct sources. Water vapor
15 181 in the eastern part of the NAM region mainly originates from the Gulf of Mexico (GoM); moisture
16 182 in Arizona appears to originate from the Gulf of California (GoC) and the eastern tropical Pacific
17 183 (Fig. 6 ; Comrie and Glenn, 1988). The moisture transport is reflected in the high surface values of
18 184 specific humidity on either side of the Mexican plateau. The elevated topography blocks and
19 185 deflects low-level winds and divides the water vapor sources with a moist tongue extending up the
20 186 Gulf of California on the west side and increased amounts of water vapor extending from the Gulf
21 187 of Mexico on the east side. Warm air over land is more buoyant and destabilizes the atmospheric
22 188 column directly above. As a result, atmospheric convection is dominant and most of the monsoonal
23 189 precipitation is convective in origin (~80-90%, Fig. 2g).

24 190 The large-scale, low-level flow over the southwestern U.S. and Mexico is strongly influenced by
25 191 the subtropical Highs (e.g., Higgins et al., 1997). The strongest flux onto the terrestrial NAM region
26 192 occurs at low levels by southeasterly and southwesterly winds. Strong northwesterly winds
27 193 associated with the large-scale circulation in the east Pacific anticyclone occur west of Baja
28 194 California (Fig. 7a). Along the west coast, the low-level flow is primarily parallel to the continent
29 195 with little influx of moisture. The large-scale, 500-hPa and 200-hPa wind fields show large
30 196 anticyclonic rotation over the southwestern U.S. (Fig. 7b, c) and steer moisture transport at lower
31 197 levels predominantly from the Gulf of Mexico.

32 198 In the following paragraphs, we are looking at the dynamics of the monsoon system during the
33 199 Eemian (125 ka) and how it differs from the present. We will discuss the changes in precipitation,
34 200 moisture and wind system averaged over the whole NAM region as well as spatial variability within
35 201 the monsoon region itself. This will allow us to better understand the underlying dynamics and
36 202 mechanisms responsible for enhanced or reduced monsoonal precipitation and to compare our
37 203 results to previous GCM studies with much lower resolution.

38
39
40
41
42
43
44
45
46
47
48
49
50
51
52
53
54
55
56
57
58
59
60

1
2
3 204 During the LIG, the overall precipitation pattern and length of the monsoon season is similar to
4 205 today with a strong summer monsoon and dry winter months. However, during the Eemian,
5 206 precipitation over the NAM region slightly increases in spring, and is considerably higher in July
6 207 and August in comparison to the present (Fig. 2e,f). Averaged over the entire monsoon region,
7 208 monthly precipitation magnitudes were about 24 mm higher in July and 14 mm higher in August.
8 209 Increased precipitation during the Eemian summer is associated with a slight increase in cloud
9 210 cover and a large increase in columnar liquid water content (Fig. 4). However, convective
10 211 precipitation changes very little (Fig. 2g), so most of the additional precipitation must be related to
11 212 large-scale phenomena. The changes in monsoonal precipitation during the Eemian were not
12 213 uniform, but indicate strong spatial variability. JJA precipitation increased by up to 60 % in the
13 214 eastern half of the monsoon region, but decreased by 35 % over Arizona in the northwestern part
14 215 of the NAM region (Fig. 5c).

15 216 The changes in the continental precipitation pattern during the Eemian can be related to changes in
16 217 tropospheric circulation and divergence fields and associated changes in monsoonal moisture
17 218 fluxes. Simulated air temperature over the GoM is slightly warmer in the Eemian compared to
18 219 modern (Fig. 3). Warmer temperatures over the GoM and along a narrow corridor from the east
19 220 coast of Mexico into New Mexico and the northern part of Arizona provides a basis for stronger
20 221 moisture transport into the eastern part of the monsoon region. Surface winds increase around 15
21 222 % over the Gulf of Mexico and the Gulf of California (Fig 7), transporting more moisture into
22 223 north-central Mexico, New Mexico and California and leading to increased evapotranspiration (4c,
23 224 d). Although moisture is concentrated in the lower troposphere over the southwestern U.S., a
24 225 change in specific humidity is also evident in the middle troposphere (Fig. 6). Higher atmospheric
25 226 moisture content at 500-hPa across the southwestern U.S. is associated with an increase in middle
26 227 and higher-level wind speeds, which appears to be a direct consequence of the northward shift of
27 228 the anticyclonic wind pattern (Fig. 7).

28 229 Although most of the monsoon region indicates an increase in precipitation during the Eemian,
29 230 Arizona shows a pronounced drying (Fig. 5c). The decrease in total precipitation over Arizona
30 231 correlates with a decrease in evapotranspiration and convection in that area (Fig. 8, 9). Most of the
31 232 precipitation over the NAM region is convective in origin, but the climatological conditions that
32 233 promote convection differ between regions (Adams and Comrie, 1997; Douglas et al., 1993). Low-
33 234 level moisture advection from the Gulf of Mexico is critical for convective activity in the eastern
34 235 part of the NAM. In the western NAM region, convection depends essentially on the presence of
35 236 lower-troposphere moisture with intense insolation and elevated topography (Adams and Souza,
36 237 2009). Simulated air temperature over the eastern subtropical Pacific and over the Gulf of

1
2
3 238 California (GoC) is colder in JJA which is in agreement with suggested Eemian cooling in the
4 239 subtropical Pacific based on Mg/Ca observational data (Leduc et al., 2010).

5
6 240 Lower air temperatures around Baja California may weaken convection (Fig. 9) and moisture
7 241 supply to the western part of the NAM region. Lower temperatures in southern Arizona correlate
8 242 with decreased evapotranspiration in the area. In addition, surface winds over Arizona are 35 %
9 243 higher in comparison to modern (Fig. 7), moving water vapor out of the area to the east. Surface
10 244 winds are from the southwest but shift from a more meridional to a more zonal direction (i.e., a
11 245 stronger western component). This could explain an increase in California precipitation, while
12 246 Arizona experiences drier conditions. Examination of the vertical structure indicates a region of
13 247 reduced upper-tropospheric (200-hPa) divergence (Suppl. 1) that coincides with reduced mid-
14 248 tropospheric vertical motion, reduced convection, and reduced monsoon rainfall in Arizona.
15
16
17
18
19
20
21

22 249

23 250 **3.4 Temporal Monsoon Variability during LIG**

24 251 Our model simulates positive temperature anomalies in early summer across the western U.S. in
25 252 response to the dominant orbital forcing mechanism that modifies the incoming solar radiation
26 253 during the early stages of the LIG. Despite similar orbital forcing configurations during the warm
27 254 phase of the LIG, the monsoonal climate during 130ka and 125ka is quite different.

28
29 255 Obliquity is largest at 130ka and peaked earlier than precession during the LIG (Crowley and Kim,
30 256 1994). The obliquity affects seasonal contrast and results in stronger monthly temperature
31 257 deviations at 130 ka than 125ka in comparison to present simulations (Fig. 2). However,
32 258 simulations show that the NAM response is dominated by precession. Positive temperature
33 259 anomalies averaged over the NAM region are significantly higher in spring at 130 ka than at 125
34 260 ka. While July temperature anomalies differ spatially under Eemian conditions, the average
35 261 temperature across the NAM region is similar to MaxObliquity. This is consistent with a shift in
36 262 perihelion from earliest May at 130 ka to late July at 125 ka and associated impacts on Northern
37 263 Hemisphere insolation (Otto-Bliesner et al., 2013).

38
39 264 The timing of perihelion increased the seasonal insolation and temperature contrast; an effect that
40 265 was amplified by the highly eccentric orbit. The effects can be seen in other climate variables. The
41 266 overall cooler temperatures in the late summer months during 130 ka taper the monsoonal response.
42 267 Averaged over the entire NAM region, MaxObliquity indicates a larger positive precipitation
43 268 anomaly in May, when insolation is the highest, but experiences an overall similar monsoon as
44 269 present, with slightly higher precipitation magnitudes in June and July (Fig. 2). JJA spatial pattern
45 270 indicate a maximum increase in precipitation of around 30-50 % in a small northeastern part of the
46 271 NAM, while large parts of Mexico indicate a modest decrease around 10-20 % or no significant
47
48
49
50
51
52
53
54
55
56
57
58
59
60

1
2
3 272 change in precipitation in comparison to today (Fig. 5d). During MaxObliquity, wind patterns
4 273 suggest an overall reduced moisture flux from both the Gulf of Mexico and the Gulf of California.
5 274 Moisture changes in the lower and middle troposphere are small in comparison to modern (Fig. 6).
6 275 Arizona experiences a similar pattern to the Eemian, with a precipitation decrease of up to 35 %.
7 276 Climate parameters over Arizona indicate a similar response as 125ka with decreasing
8 277 evapotranspiration and convection in the area.

9 278 While we are mainly focusing on the warm periods of the early LIG, we want to present a short
10 279 summary of climate changes related to MinObliquity in order to provide a comparison in
11 280 monsoonal variability in relation to orbital parameters. Eccentricity is large throughout the entire
12 281 LIG. With minimum obliquity and perihelion in January, seasonal contrasts at 115 ka are moderate.
13 282 In response to lower insolation and lower temperature in spring and summer, the NAM region is
14 283 slightly dryer with precipitation about 5 to 10 % lower than modern. The decrease in total
15 284 precipitation is mostly due to a slight decrease in convection and associated less intense storm
16 285 events throughout the summer. MinObliquity is characterized by a strong reduction in moisture at
17 286 the lower and middle troposphere. The extent and magnitude of drying is similar to the spatial
18 287 pattern observed for increased humidity in the Eemian. Maximum decrease in surface moisture is
19 288 observed in the NAMEast region and north of the core monsoon, while moisture in the middle
20 289 troposphere mostly decreases in southern California (Fig. 6). The upper level anticyclone weakens
21 290 and shifts southeast.

22 291

23 292

24 293 **4. Discussion**

25 294 Overall, our simulations suggest a temporally and spatially diverse response to insolation changes
26 295 in the North American Monsoon region. We contribute the difference in the timing and magnitude
27 296 of maximum insolation and temperature changes to changes in obliquity and precession. Previous
28 297 studies (e.g., Bakker et al., 2013; Otto-Bliesner et al., 2013) have shown that the radiative forcing
29 298 provided by the changes in the three major GHGs is small ($< 0.2 \text{ W m}^{-2}$) compared to the forcing
30 299 provided by the insolation changes. Our simulated June and July temperatures are consistent with
31 300 results from earlier model inter-comparison studies that show robust Northern Hemisphere July
32 301 temperature evolution characterized by a maximum between 130 – 125 ka with temperatures 0.3 to
33 302 5.3 K above pre-present day (Bakker et al., 2013; Lunt et al., 2013). Proxy datasets of quantitative
34 303 estimates of mean annual surface temperatures only include a limited number of terrestrial sites in
35 304 the U.S. However, intact Eemian wood samples have been recovered from sediments of the Ziegler
36 305 Reservoir in Snowmass Colorado (Pigati et al., 2014). A unit corresponding to MIS 5e has been

1
2
3 306 dated to between ~126 and 120 ka with mean July temperature reconstruction that have been similar
4 307 to or slightly warmer than they are today (Elias, 2014). Interestingly, the core region of the NAM
5 308 region, including northwestern Mexico and southwestern Arizona, indicates cooling in July and
6 309 August. We attribute this pattern to increased cloud cover and an increase in total columnar liquid
7 310 water content (Fig. 4a, b). The clouds tend to have a negative radiative forcing. While the TOA
8 311 insolation is significantly higher during the early LIG, the surface net downward shortwave flux is
9 312 similar to modern in July and August. This pattern is consistent with previous model results that
10 313 show continental cooling at subtropical northern latitudes associated with the core regions of other
11 314 monsoon systems such as Asian and African systems (Otto-Bliesner et al., 2013).
12 315 Our model indicates northward movement of the mid-level anticyclone and warming over the Gulf
13 316 of Mexico that facilitates stronger moisture transport into the eastern NAM region. An
14 317 intensification of precipitation over most of the southwestern U.S. during the Eemian is consistent
15 318 with previous studies that suggest a more intense NAM in response to increased Northern
16 319 Hemisphere insolation (Asmerom et al., 2007; Barron et al., 2012; Metcalfe et al., 2015). A recent
17 320 study by Scussolini et al. (2019) compares simulated hydroclimates in LIG model experiments with
18 321 proxy data and explores the limitations of data-model comparisons. In very good agreement with
19 322 our simulation, Scussolini's model ensemble shows higher average precipitation of the NAM
20 323 during the early LIG by about 34%. The models used in that study indicate considerable variability
21 324 with the EC-Earth model suggesting a slight decrease in monsoonal precipitation during the LIG
22 325 (Scussolini et al., 2019). Very few terrestrial LIG proxies exist in the southwestern U.S. and none
23 326 of them unambiguously project seasonal precipitation anomalies. Multiproxy data from wetland
24 327 records in Colorado (Miller et al., 2014) and pollen proxies from ancient lakes in California
25 328 (Bradbury, 1997; Ku et al., 1998; Menking et al., 1997; Reheis et al., 2012) suggest overall wetter
26 329 conditions during the early LIG, but it is not clear whether these anomalies are related to summer
27 330 or winter precipitation.
28 331 Our model predicts an increase in monsoonal precipitation over most parts of the southwestern
29 332 U.S., but also distinctively drier conditions over the northwest corner of the core monsoonal area
30 333 in Arizona. We are not aware of datasets that can verify or refuse the idea of regional drying in
31 334 parts of the NAM during the Eemian. Paleoclimate model simulations are usually conducted with
32 335 lower-resolution general circulation models that provide large-scale information, but do not resolve
33 336 small-scale regional variations. However, the proposed spatial variability in monsoonal
34 337 precipitation is consistent with the dual nature of the modern monsoon, where anomalously wet
35 338 periods in New Mexico do correspond to low precipitation periods in Arizona or vice versa,
36
37
38
39
40
41
42
43
44
45
46
47
48
49
50
51
52
53
54
55
56
57
58
59
60

1
2
3 339 supporting the evidence of different moisture sources and paths for the two regions (Comrie and
4 340 Glenn, 1998).

5
6 341 The climate of the Eemian is closely related to the orbital forcing configurations that result in a
7 342 pronounced seasonal cycle with warmer summers and colder winters. Current and future climate
8 343 change is associated with greenhouse gas radiative forcing that will most likely result in uniformly
9 344 warm conditions throughout the year. While the difference in forcing factors might limit our
10 345 expectations of a direct comparison between the two warming scenarios, positive temperature
11 346 anomalies and associated patterns in hydroclimate have been proposed in future climate
12 347 projections. There is observational evidence to suggest that monsoon precipitation is becoming
13 348 more extreme in the Southwest and northwestern Mexico with increasing surface temperatures
14 349 (Anderson et al., 2010; Chang et al., 2015; Luong et al., 2017). An overall stronger monsoon can
15 350 be explained by strong feedbacks between insolation, evapotranspiration, convection, and
16 351 cloudiness. However, summertime convective activity in the southwestern U.S. is spatially variable
17 352 and results from complex interactions between atmospheric circulation features and the complex
18 353 topography (Adams and Souza, 2009). Drier conditions in Arizona may reflect local topographic
19 354 effects that are critical to the distribution of convective activity. Adams and Comrie (1997)
20 355 discussed the formation of the NAM in response to temperature contrasts between seasonally warm
21 356 low land surfaces and elevated areas together with atmospheric moisture supply from nearby
22 357 maritime source. In the modern context, the thermal contrast in the Gulf of California facilitates
23 358 the formation of moisture-laden air masses that move northward toward a region of low pressure
24 359 centered over Arizona (Pascale and Bordoni, 2016; Wu et al., 2009). Our simulations show a
25 360 decrease in temperature in the low-lying regions of Arizona, which reduces the thermal low and
26 361 reduces convective precipitation (Fig. 5, 8). Our results are in agreement with Pascal et al. (2017)
27 362 who highlights the possibility of a strong precipitation reduction in the northwestern edge of the
28 363 monsoon region in response to increased atmospheric stability and weakened convection with
29 364 increasing temperatures.

30
31
32
33
34
35
36
37
38
39
40
41
42
43
44 365 Here, we propose an additional mechanism that might contribute to a spatially variable precipitation
45 366 pattern. The western NAM region experiences the highest precipitation flux in late August to early
46 367 September, in contrast to the July precipitation maximum in the eastern NAM region. This pattern
47 368 may reflect an enhanced influence of tropical Pacific cyclones on precipitation in late summer
48 369 (Corbosiero et al., 2009; Englehart and Douglas, 2001; Ritchie et al., 2011). Arizona experiences
49 370 the highest contribution of tropical cyclone remnants to warm-season precipitation (~15-25%;
50 371 Ritchie et al., 2011). During the Eemian, a decrease in eastern Pacific winds along the coast of Baja
51 372 California and the northward shift of the upper-level anticyclone (Fig. 7) may allow a more
52
53
54
55
56
57
58
59
60

1
2
3 373 north/northwest path of tropical Pacific cyclones, resulting in higher precipitation in Mexico and/or
4 374 California and Nevada, but reduced rainfall over Arizona (consistent with the group 3 and 4 tropical
5 375 cyclone remnants as described by (Ritchie et al., 2011). In this case, precipitation can increase along
6 376 the west coast of the southwestern U.S., but the topography of southern California and the Sierra
7 377 Nevada limits penetration of Pacific moisture (Adams and Comrie, 1997), thus resulting in drier
8 378 conditions over Arizona. Current and future climate projections suggest cyclone intensification in
9 379 response to a warmer climate (e.g., Balaguru et al., 2018; Bathia et al., 2019; Holland and Bruyère,
10 380 2014; Walsh et al., 2016), but it is difficult to simulate hurricane distribution in the past, mostly
11 381 due to uncertainties in sea surface temperatures and the time-scale involved (Frappier et al., 2007).
12 382 However, warmer temperatures and a shift in large-scale circulation during the Eemian may have
13 383 had the potential to increase the tropical cyclone contribution to NAM precipitation in late summer.
14 384 It is important to note that most of the NAM literature has a strong geographical bias toward the
15 385 state of Arizona, but differences in precipitation response between the eastern and western NAM
16 386 regions are very apparent in our model output as well as modern observations (Comrie and Glenn,
17 387 1998). Our model simulations suggest that in a warmer climate, NAM regions that are dominated
18 388 by local convection experience drier conditions, while regions that can pick up large-scale systems,
19 389 either through enhanced moisture transport from the Gulf of Mexico or increased impact of tropical
20 390 storms, experience wetter conditions. Our findings are consistent with present-day analysis from
21 391 the Climate Prediction Center and individual Cooperative Observer Program (COOP) stations with
22 392 long-term records of precipitation in the southwestern U.S. that indicate a significant increase in
23 393 mean precipitation in New Mexico, but a decrease in mean monsoon precipitation over Arizona in
24 394 recent decades (Luong et al., 2017).

25 395 The precipitation response to increased solar radiation and associated warming is complex. The
26 396 NAM region does not experience a uniform response to changing climate conditions. A more
27 397 detailed analysis with high-resolution models (<25 to 10km resolution) is necessary to account for
28 398 a thorough analysis of the Gulf of California response to insolation changes. We may not accurately
29 399 resolve the summertime low-level flow along the Gulf of California which may impact precipitation
30 400 estimates in the southwestern US. However, our model results are in good agreement with previous
31 401 studies trying to unravel the NAM history in response to warmer interglacial periods as well as
32 402 modern observations in a warming climate.

33 403

34 404

35 405 **Acknowledgements:**

36

37

38

39

40

41

1
2
3 406 This study was supported by the National Science Foundation grant NSF EAR 1502772. The work
4 407 was completed in part with resources and assistance provided by the University of Chicago
5 408 Research Computing Center. We thank two anonymous reviewers for constructive comments on
6 409 the manuscript.
7
8
9

10 410

11 411 **Figures:**

12 412 Figure 1: Measured and simulated monsoonal precipitation across North America. (a) Precipitation
13 413 (in percent of annual precipitation) during the peak NAM season (July, August, September = JAS)
14 414 based on observations from the Global Precipitation Climatology Centre (GPCC) database from
15 415 1981 to 2010. (b) RegCM4 simulated 10-year mean JAS precipitation. Red box highlights the main
16 416 NAM monsoon region, green box indicates Arizona ‘dry’ region (see text for explanation). (c)
17 417 Monthly precipitation flux of observed and simulated precipitation over the monsoon region.
18
19
20
21
22

23 418

24 419 Figure 2: Simulated forcing factors and climatic indices averaged over the North American
25 420 Monsoon region for 4 cases: modern (black line), 115 ka (blue line), 125ka (green line), and 130
26 421 ka (red line). (a) Incoming solar radiation at the top of the atmosphere indicates higher incoming
27 422 shortwave flux during the early LIG. (b) Surface net shortwave flux highlights cloud feedbacks
28 423 during the summer months. (c) Surface temperature and highlighted differences in temperature
29 424 between case study and modern. (e) and (f) Total precipitation and difference in precipitation
30 425 between case study and modern. (g) Convective precipitation. Large differences in total
31 426 precipitation, but small differences in convective precipitation during the Eemian highlights the
32 427 impact of additional large-scale transport of moisture into the study area.
33
34
35
36
37
38

39 428

40 429 Figure 3: Simulated temperature differences between LIG and modern from May to August. Top
41 430 row: Difference in temperature between MinObliquity and modern. Middle row: Temperature
42 431 differences between Eemian and modern. Bottom row: Temperature difference between
43 432 MaxObliquity and modern. The monthly maps indicate surface temperature with fixed ocean
44 433 temperature. Notice lower temperatures in July and August in the NAM region. The right column
45 434 shows near surface air temperature differences averaged over June, July, August. Although sea
46 435 surface temperatures have been held constant in the model, the air temperature increases over the
47 436 Gulf of Mexico and decreases over the Gulf of California during the Eemian and 130 ka.
48
49
50
51
52

53 437

54 438 Figure 4: Simulated forcing factors and climate variable averaged over the North American
55 439 Monsoon region for 4 cases: modern (black line), 115 ka (blue line), 125ka (green line), and 130
56
57
58
59
60

1
2
3 440 ka (red line). (a) Total cloud fraction (b) Total liquid water content. (c) and (d) Total
4 441 evapotranspiration flux and difference in evapotranspiration between case studies and modern.
5 442 All graphs indicate an increase in atmospheric moisture during the early LIG.
6
7

8 443
9 444 Figure 5: Simulated precipitation differences (in percentage) between LIG and modern for July,
10 445 August, September (JAS). (a) Simulated JAS precipitation (in mm/day) over the U.S. (b)
11 446 Difference in precipitation between MinObliquity and modern; (c) Precipitation differences
12 447 between Eemian and modern; (d) Precipitation difference between MaxObliquity and modern.
13 448 Notice strong duality pattern between Arizona and eastern monsoon region during 125 ka.
14
15
16
17

18 449
19 450 Figure 6: Distribution of specific humidity averaged over JAS. (a) Surface moisture; (b-d)
20 451 Difference in surface specific humidity between LIG case studies and modern; (e) Modern humidity
21 452 at 500 hPa. Map view shows distinct moisture sources for Arizona and New Mexico; (f-h) Humidity
22 453 difference at 500 hPa between LIG case studies and modern. Notice the increase in humidity at
23 454 different atmospheric levels during the Eemian.
24
25
26

27 455
28 456 Figure 7: Wind patterns averaged over JAS in the Modern and during the Eemian. (a-c) Modern
29 457 winds at the surface, 500-hPa, and 200-hPa. The model realistically simulates the anticyclonic
30 458 patterns at mid- and high-levels. (d-e) Vectors are showing difference in wind magnitude under
31 459 Eemian and modern conditions. Vector colors indicate magnitude, positive and negative signs are
32 460 related to the change in physical direction of winds.
33
34
35

36 461
37 462 Figure 8: Simulated climate variables averaged over southern Arizona for 4 cases: modern (black
38 463 line), 115 ka (blue symbols), 125 ka (green line), and 130 ka (red symbols). (a-c) Total
39 464 precipitation, precipitation difference, and convective precipitation. Precipitation is decreasing
40 465 during the Eemian summer months across southern Arizona. (d-e) Total evapotranspiration flux
41 466 an difference in evapotranspiration between case studies and modern.
42
43
44
45

46 467
47 468 Figure 9: Vertical velocity (ω) across the NAM domain at around 32N during JAS.
48 469 Height/pressure-longitudinal profile with negative values indicating strong upward air
49 470 component. (a) Modern simulations. (b) Simulations with Eemian boundary conditions. Notice
50 471 the reduction in vertical velocity on the western side (southern Arizona).
51
52
53
54

55 472
56 473 Table 1: Forcings and boundary conditions used in RegCM simulations.
57
58
59
60

1
2
3
4
5
6
7
8
9
10
11
12
13
14
15
16
17
18
19
20
21
22
23
24
25
26
27
28
29
30
31
32
33
34
35
36
37
38
39
40
41
42
43
44
45
46
47
48
49
50
51
52
53
54
55
56
57
58
59
60

474

475 Supplement Figure 1: Difference in moisture and upper-level divergence between Eemian and
476 modern.

477

478

479 Bibliography:

- 480 Adams, D.K. and Comrie, A.C., 1997. The North American Monsoon. *Bulletin of the American*
481 *Meteorological Society*, 78(10): 2197-2213.
- 482 Adams, D.K. and Souza, E.P., 2009. CAPE and Convective Events in the Southwest during the
483 North American Monsoon. *Monthly Weather Review*, 137(1): 83-98.
- 484 Anderson, B.T., Wang, J., Salvucci, G., Gopal, S. and Islam, S., 2010. Observed Trends in
485 Summertime Precipitation over the Southwestern United States. *Journal of Climate*,
486 23(7): 1937-1944.
- 487 Asmerom, Y., Polyak, V., Burns, S. and Rasmussen, J., 2007. Solar forcing of Holocene climate:
488 New insights from a speleothem record, southwestern United States. *Geology*, 35(1): 1.
- 489 Bakker, P., Stone, E.J., Charbit, S., Groeger, M., Krebs-Kanzow, U., Ritz, S.P., Varma, V., Khon,
490 S., Lunt, D.J., Mikolajewicz, U., Prange, M., Renssen, H., Schneider, B. and Schulz, M.,
491 2013. Last interglacial temperature evolution - a model inter-comparison. *Climate of the*
492 *Past Discussions*, 8: 4663-4699.
- 493 Balaguru, K., Foltz, G.R. and Leung, L.R., 2018. Increasing Magnitude of Hurricane Rapid Intensification in the Central and
494 Eastern Tropical Atlantic. *Geophysical Research Letter*, 45(9): 4238-4247.
- 495 Bard, E., Hamelin, B. and Fairbanks, R.G., 1990. U-Th ages obtained by mass spectrometry in
496 corals from Barbados: sea level during the past 130,000 years. *Nature*, 346: 456- 458.
- 497 Barron, J.A., Metcalfe, S.E. and Addison, J.A., 2012. Response of the North American monsoon
498 to regional changes in ocean surface temperature. *Paleoceanography*, 27.
- 499 Bathia, K., Vecchi, G.A., Knutson, T.R., Murakami, H., Kossin, J., Dixon, K.W. and Whitlock,
500 C.E., 2019. Recent increases in tropical cyclone intensification rates. *Nature*
501 *Communications*.
- 502 Berger, A. and Loutr, A.F., 1991. Insolation Values for the Climate of the Last 10 Million Years.
503 *Quaternary Science Reviews*, 10: 297 - 317.
- 504 Bradbury, J.P., 1997. A Diatom Record of Climate and Hydrology for the past 200 ka from
505 Owens Lake, California with Comparison to Other Great Basin Records. *Quaternary*
506 *Science Reviews*, 16: 203-219.
- 507 Brown, P.M., Nash, S.E. and Kline, D., 2014. Identification and dendrochronology of wood
508 found at the Ziegler Reservoir fossil site, Colorado, USA. *Quaternary Research*, 82(3):
509 575-579.
- 510 CAPE members - Anderson, P., Bennike, O., Bigelow, N., Brigham-Grette, J., Divall, M.,
511 Edwards, M., Frechette, 2006. Last Interglacial Arctic warmth confirms polar
512 amplification of climate change. *Quaternary Science Reviews*, 25(13-14): 1383-1400.
- 513 Chang, H.I., Castro, C.L., Carrillo, C.M. and Dominguez, F., 2015. The more extreme nature of
514 U.S. warm season climate in the recent observational record and two “well - performing
515 ” dynamically downscaled CMIP3 models. *Journal of Geophysical Research:*
516 *Atmospheres*, 120(16): 8244-8263.
- 517 Comrie, A.C. and Glenn, E.C., 1998. Principle components-based regionalization of precipitation
518 regimes across the southwest United States and northern Mexico, with an application to
519 monsoon precipitation variability. *Climate Research*, 10: 201 - 215.

- 1
2
3 520 Cook, B.I. and Seager, R., 2013. The response of the North American Monsoon to increased
4 521 greenhouse gas forcing. *118*(4): 1690-1699.
- 5 522 Corbosiero, K.L., Dickinson, M.J. and Bosart, L.F., 2009. The Contribution of Eastern North
6 523 Pacific Tropical Cyclones to the Rainfall Climatology of the Southwest United States.
7 524 *Monthly Weather Review*, 137(8): 2415-2435.
- 8 525 Crowley, T.J. and Kim, K.-Y., 1994. Milankovitch Forcing of the Last Interglacial Sea Level.
9 526 *Science*, 265(5178): 1566-1568.
- 10 527 Cruz, F.W., Jr, Burns, S., J., Karmann, I., Sharp, W.D., Vuille, M., Cardoso, A.O., Ferrari, J.A.,
11 528 Silva Dias, P.L. and Vlana Jr, O., 2005. Insolation-driven changes in atmospheric
12 529 circulation over the past 116,000 years in subtropical Brazil. *Nature*, 434: 63 - 66.
- 13 530 Cuffey, K.M. and Marshall, S.J., 2000. Substantial contribution to sea-level rise during the last
14 531 interglacial from the Greenland ice sheet. *Nature*, 404: 591 - 594.
- 15 532 Diem, J.E., Brown, D.P. and McCann, J., 2013. Multi-decadal changes in the North American
16 533 monsoon anticyclone. *International Journal of Climatology*, 33(9): 2274-2279.
- 17 534 Diffenbaugh, N.S., Ashfaq, M., Shuman, B., Williams, J.W. and Bartlein, P.J., 2006. Summer
18 535 aridity in the United States: Response to mid-Holocene changes in insolation and sea
19 536 surface temperature. *Geophysical Research Letters*, 33(22).
- 20 537 Diro, G.T., Rauscher, S.A., Giorgi, F. and Tomkins, A.M., 2012. Sensitivity of seasonal climate
21 538 and diurnal precipitation over Central America to land and sea surface schemes in
22 539 RegCM4. *Climate Research* 2: 31-48.
- 23 540 Douglas, M.W., Maddox, R.A., Howard, K. and Reyes, S., 1993. The Mexican Monsoon. *Journal*
24 541 *of Climate*, 6: 1665-1667.
- 25 542 Elias, S.A., 2014. Environmental interpretation of fossil insect assemblages from MIS 5 at Ziegler
26 543 Reservoir, Snowmass Village, Colorado. *Quaternary Research*, 82(3): 592-603.
- 27 544 Emanuel, K.A., 1991. A Scheme for Representing Cumulus Convection in Large-Scale Models.
28 545 *Journal of the Atmospheric Sciences*, 48(21): 2313-2329.
- 29 546 Englehart, P.J. and Douglas, A.V., 2001. The role of eastern North Pacific tropical storms in the
30 547 rainfall climatology of western Mexico. *International Journal of Climatology*, 21(11):
31 548 1357-1370.
- 32 549 Frappier, A., Knutson, T., Liu, K.-B. and Emanuel, K., 2007. Perspective: coordinating
33 550 paleoclimate research on
34 551 tropical cyclones with hurricane-climate theory
35 552 and modelling. *Tellus*, 59A: 529-537.
- 36 553 Fuentes-Franco, R., Coppola, E., Giorgi, F., Graef, F. and Pavia, E.G., 2014. Assessment of
37 554 RegCM4 simulated inter-annual variability and daily-scale statistics of temperature and
38 555 precipitation over Mexico. *Climate Dynamics*, 42: 629-647.
- 39 556 Giorgi, F., Coppola, E., Solmon, F., Mariotti, L., Sylla, M., Bi, X., Elguindi, N., Diro, G., Nair,
40 557 V., Giuliani, G., Turuncoglu, U., Cozzini, S., Güttler, I., O'Brien, T., Tawfik, A.,
41 558 Shalaby, A., Zakey, A., Steiner, A., Stordal, F., Sloan, L. and Brankovic, C., 2012.
42 559 RegCM4: model description and preliminary tests over multiple CORDEX domains.
43 560 *Climate Research*, 52: 7-29.
- 44 561 Giorgi, F., Marinucci, M.R. and Bates, G.T., 1993a. Development of a Second-Generation
45 562 Regional Climate Model (RegCM2). Part I: Boundary-Layer and Radiative Transfer
46 563 Processes. *Monthly Weather Review*, 121(10): 2794-2813.
- 47 564 Giorgi, F., Marinucci, M.R., Bates, G.T. and De Canio, G., 1993b. Development of a Second-
48 565 Generation Regional Climate Model (RegCM2). Part II: Convective Processes and
49 566 Assimilation of Lateral Boundary Conditions. *Monthly Weather Review*, 121(10): 2814-
50 567 2832.
- 51 568 Grell, G.A., Dudhia, J. and Stauffer, D.R., 1994. A Description of the Fifth-Generation
52 569 PennState/NCAR Mesoscale Model (MM5). NCAR technical report, TN-398+STR: p
53 570 121.
- 54
55
56
57
58
59
60

1
2
3
4
5
6
7
8
9
10
11
12
13
14
15
16
17
18
19
20
21
22
23
24
25
26
27
28
29
30
31
32
33
34
35
36
37
38
39
40
41
42
43
44
45
46
47
48
49
50
51
52
53
54
55
56
57
58
59
60

- 571 Griffin, D., Woodhouse, C.A., Meko, D.M., Stahle, D.W., Faulstich, H.L., Carrillo, C., Touchan,
572 R., Castro, C.L. and Leavitt, S.W., 2013. North American monsoon precipitation
573 reconstructed from tree-ring latewood. *Geophysical Research Letters*, 40(5): 954-958.
- 574 Higgins, R.W., Yao, Y. and X.L. W., 1997. Influence of the North American Monsoon System on
575 the U.S. Summer Precipitation Regime. *Journal of Climate*, 10: 2600 - 2622.
- 576 Holland, G. and Bruyère, C.L., 2014. Recent intense hurricane response to global climate change.
577 *Climate Dynamics*, 42: 617-627.
- 578 Insel, N., Poulsen, C. and Ehlers, T., 2009. Influence of the Andes Mountains on South American
579 moisture transport, convection, and precipitation. *Climate Dynamics*, 35: 1477-1492.
- 580 Kleinen, T., Brovkin, V. and Munhoven, G., 2016. Modelled interglacial carbon cycle dynamics
581 during the Holocene, the Eemian and Marine Isotope Stage (MIS) 11. *Climate of the*
582 *Past*, 12(12): 2145-2160.
- 583 Ku, T.-L., Luo, S., Lowenstein, T.K., Li, J. and Spencer, R., 1998. U-Series Chronology of
584 Lacustrine Deposits in Death Valley, California. *Quaternary Research*, pp. 261-275.
- 585 Kukla, G.J., Bender, M.L., de Beaulieu, J.-L., Bond, G. and Broecker, W.S., 2002. Last
586 Interglacial Climates. *Quaternary Research*, 58: 2-13.
- 587 Kutzbach, J.E. and Liu, Z., 1997. Response of the African Monsoon to Orbital Forcing and Ocean
588 Feedbacks in the Middle Holocene. *Science*, 278(5337): 440-443.
- 589 Leduc, G., Schneider, R., Kim, J.H. and Lohmann, G., 2010. Holocene and Eemian sea surface
590 temperature trends as revealed by alkenone and Mg/Ca paleothermometry. *Quaternary*
591 *Science Reviews*, 29(7-8): 989-1004.
- 592 Liu, X., Liu, Z., Kutzbach, J.E., Clemens, S.C. and Prell, W.L., 2006. Hemispheric Insolation
593 Forcing of the Indian Ocean and Asian Monsoon: Local versus Remote Impacts.
594 *American Meteorological Society*, 19: 6195 - 6208.
- 595 Lunt, D.J., Abe-Ouchi, A., Bakker, P., Berger, A., Braconnot, P., Charbit, P., Fischer, N., Herold,
596 N., Jungclauss, J.H., Khon, V.C., Krebs-Kanzow, U., Langebroek, P.M., Lohmann, G.,
597 Nisancioglu, K.H., Otto-Bliesner, B.L., Park, W., Pfeiffer, M., Phipps, S.J., Prange, M.,
598 Rachmayani, R., Renssen, H., Rosenbloom, N., Schneider, B., Stone, E.J., Takahashi, K.,
599 Wei, W., Yin, Q. and Zhang, Z.S., 2013. A multi-model assessment of last interglacial
600 temperatures. *Climate of the Past*, pp. 699-717.
- 601 Luong, T.M., Castro, C.L., Chang, H.-I., Lahmers, T., Adams, D.K. and Ochoa-Moya, C.A.,
602 2017. The More Extreme Nature of North American Monsoon Precipitation in the
603 Southwestern United States as Revealed by a Historical Climatology of Simulated Severe
604 Weather Events. *Journal of Applied Meteorology and Climatology*, 56(9): 2509-2529.
- 605 McKay, N.P., Overpeck, J.T. and Otto-Bliesner, B.L., 2011. The role of ocean thermal expansion
606 in Last Interglacial sea level rise. *Geophysical Research Letters*, 38(14): n/a-n/a.
- 607 Menking, K.M., Bischoff, J.L., Fitzpatrick, J.A., Burdette, J.W. and Rye, R.O., 1997. Oscillations
608 since 155,000 yr BP at Owens Lake, California, Reflected in Abundance and Stable
609 Isotope Composition of Sediment Carbonate. *Quaternary Research*, pp. 58-68.
- 610 Metcalfe, S.E., Barron, J.A. and Davies, S.J., 2015. The Holocene history of the North American
611 Monsoon: 'known knowns' and 'known unknowns' in understanding its spatial and
612 temporal complexity. 120: 1-27.
- 613 Miller, D.M., Miller, I., M. and Jackson, S.T., 2014. Biogeography of Pleistocene conifer species
614 from the Ziegler Reservoir fossil site, Snowmass Village, Colorado. *Quaternary*
615 *Research*, 82: 567-574.
- 616 Montoya, M., von Storch, H. and Crowley, T.J., 2000. Climate Simulation for 125 kyr BP with a
617 Coupled Ocean-Atmosphere General Circulation Model. *Journal of Climate*, 13: 1058 -
618 1072.
- 619 Otto-Bliesner, B.L., Rosenbloom, N., Stone, E.J., McKay, N.P., Lunt, D.J., Brady, E.C. and
620 Overpeck, J.T., 2013. How warm was the last interglacial? New model-data comparisons.
621 *Philos Trans A Math Phys Eng Sci*, 371(2001): 20130097.

- 1
2
3 622 Pal, J.S., Giorgi, F., Bi, X., Elguindi, N., Solmon, F., Rauscher, S.A., Gao, X., Francisco, R.,
4 623 Zakey, A., Winter, J., Ashfaq, M., Syed, F.S., Sloan, L.C., Bell, J.L., Diffenbaugh, N.S.,
5 624 Karmacharya, J., Konaré, A., Martinez, D., Da Rocha, R.P. and Steiner, A.L., 2007.
6 625 Regional Climate Modeling for the Developing World: The ICTP RegCM3 and
7 626 RegCNET. 88(9): 1395-1409.
- 8 627 Pascale, S., Boos, W.R., Bordoni, S., Delworth, T.L., Kapnick, S.B., Murakami, H., Vecchi, G.A.
9 628 and Zhang, W., 2017. Weakening of the North American monsoon with global warming.
10 629 Nature Climate Change, 7(11): 806-812.
- 11 630 Pascale, S. and Bordoni, S., 2016. Tropical and Extratropical Controls of Gulf of California
12 631 Surges and Summertime Precipitation over the Southwestern United States. Monthly
13 632 Weather Review, 144(7): 2695-2718.
- 14 633 Pigati, J.S., Miller, I.M., Johnson, K.R., Honke, J.S., Carrara, P.E., Muhs, D.R., Skipp, G. and
15 634 Bryant, B., 2014. Geologic setting and stratigraphy of the Ziegler Reservoir fossil site,
16 635 Snowmass Village, Colorado. Quaternary Research, 82(3): 477-489.
- 17 636 Poore, R.Z., Pavich, M.J. and Grissino-Mayer, H.D., 2005. Record of the North American
18 637 southwest monsoon from Gulf of Mexico sediment cores. Geology, 33(3).
- 19 638 Reheis, M., J, B., SP, L., DM, M., G, S. and RJ, F., 2012. A half-million-year record of
20 639 paleoclimate from the Lake Manix Core, Mojave Desert, California. .
21 640 Palaeogeography, Palaeoclimatology, Palaeoecology, 365-366: 11-37.
- 22 641 Reynolds, R.W., Rayner, N.A., Smith, T.M., Stokes, D.C. and Wang, W., 2002. An Improved In
23 642 Situ and Satellite SST Analysis for Climate. Journal of Climate, 15(13): 1609-1625.
- 24 643 Ritchie, E.A., Wood, K.M., Gutzler, D.S. and White, S.R., 2011. The Influence of Eastern Pacific
25 644 Tropical Cyclone Remnants on the Southwestern United States. Monthly Weather
26 645 Review, 139(1): 192-210.
- 27 646 Schneider, U., Becker, A., Finger, P., Meyer-Christoffer, A., Rudolf, B. and Ziese, M., 2011.
28 647 GPCP Full Data Reanalysis Version 6.0 at 0.5°: MONTHLY Land-Surface Precipitation
29 648 from Rain-Gauges built on GTS-based and Historic Data.
- 30 649 Scussolini, P., Bakker, P., Guo, C., Stepanek, C., Zhang, Q., Braconnot, P., Cao, J., Guarino, M.-
31 650 V., Coumou, D., Prange, M., Ward, P.J., Renssen, H., Kageyama, M., Otto-Bliesner, B.
32 651 and Aerts, J.C.J.H., 2019. Agreement between reconstructed and modeled boreal
33 652 precipitation of the Lat Interglacial. Science Advances, 5(11).
- 34 653 Sinha, P., Maurya, R.K.S., Mohanty, M.R. and Mohanty, U.C., 2019. Inter-comparison and
35 654 evaluation of mixed-convection schemes in RegCM4 for Indian summer monsoon
36 655 simulation. Atmospheric Research, 215: 239-252.
- 37 656 Strickland, L.E., Baker, R.G., Thompson, R.S. and Miller, D.M., 2014. Last interglacial plant
38 657 macrofossils and climates from Ziegler Reservoir, Snowmass Village, Colorado, USA.
39 658 Quaternary Research, 82(3): 553-566.
- 40 659 Sylla, M.B., Coppola, E., Mariotti, L., Giorgi, F., Ruti, P., Dell'Aquila, A. and Bi, X., 2010.
41 660 Multiyear simulation of the African climate using a regional climate model (RegCM3)
42 661 with the high resolution ERA-interim reanalysis. Climate Dynamics, 35: 231-247.
- 43 662 Turney, C.S.M. and Jones, R.T., 2010. Does the Agulhas Current amplify global temperatures
44 663 during super-interglacials? Journal of Quaternary Science, 25(6): 839-843.
- 45 664 Velikou, K. and Tolika, K., 2017. Evaluation of the Sensitivity of the Updated RegCM4 Model to
46 665 Physics Parameterizations over the Mediterranean Region: Precipitation and Temperature
47 666 Simulations. Proceedings, 1(112).
- 48 667 Walsh, K.J., McBride, J.L., Klotzbach, P.J., Balachandran, S., Camargo, S.J., Holland, G.,
49 668 Knutson, T.R., Kossin, J.P., Lee, T.c., Sobel, A. and Sugi, M., 2016. Tropical cyclones
50 669 and climate change. WIREs Clim Change, 7: 65-89.
- 51 670 Wang, Y.J., Cheng, H., Edwards, R.L., An, Z.S., Wu, J.Y., Shen, C.-C. and Dorale, J.A., 2001. A
52 671 High-Resolution Absolute-Dated Late Pleistocene Monsoon Record from Hulu Cave,
53 672 China. Science(5550): 2345-2348.
- 54
55
56
57
58
59
60

1
2
3
4
5
6
7
8
9
10
11
12
13
14
15
16
17
18
19
20
21
22
23
24
25
26
27
28
29
30
31
32
33
34
35
36
37
38
39
40
41
42
43
44
45
46
47
48
49
50
51
52
53
54
55
56
57
58
59
60

673 Wu, M.-L.C., Schubert, S.D., Suarez, M.J. and Huang, N.E., 2009. An Analysis of Moisture
674 Fluxes into the Gulf of California. *Journal of Climate*, 22(8): 2216-2239.
675 Zhong, Z., Hu, Y., Min, J. and Xu, H., 2007. Numerical Experiments on the Spin-up Time for
676 Seasonal-Scale Regional Climate Modeling. *Acta Meteorologica Sinica*, 21(4): 409-419.
677

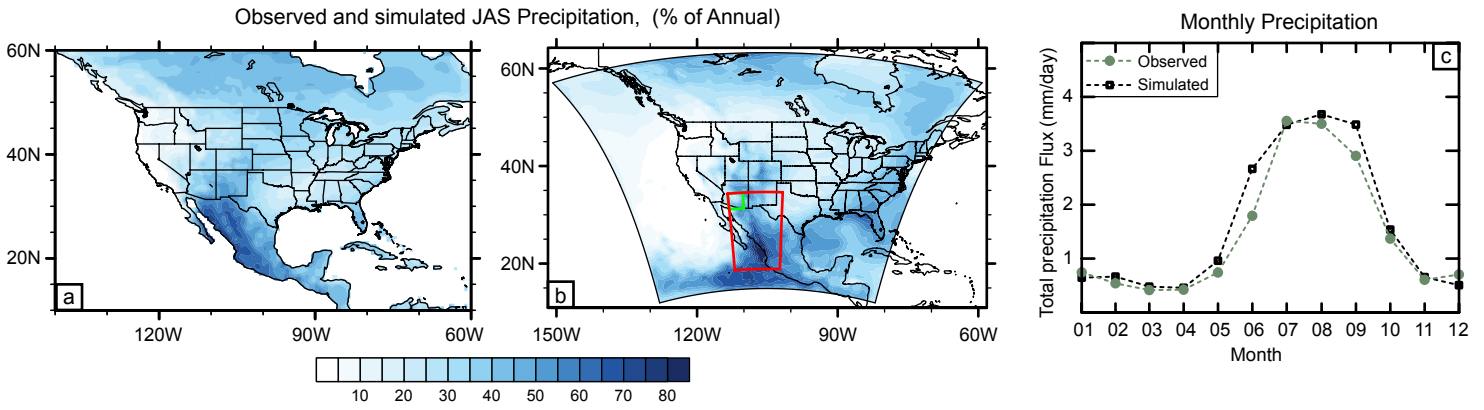


Figure 1: Measured and simulated monsoonal precipitation across North America. (a) Precipitation (in percent of annual precipitation) during the peak NAM season (July, August, September = JAS) based on observations from the Global Precipitation Climatology Centre (GPCC) database from 1981 to 2010. (b) RegCM4 simulated 10-year mean JAS precipitation. Red box highlights the main NAM monsoon region, green box indicates Arizona 'dry' region (see text for explanation). (c) Monthly precipitation flux of observed and simulated precipitation over the monsoon region.

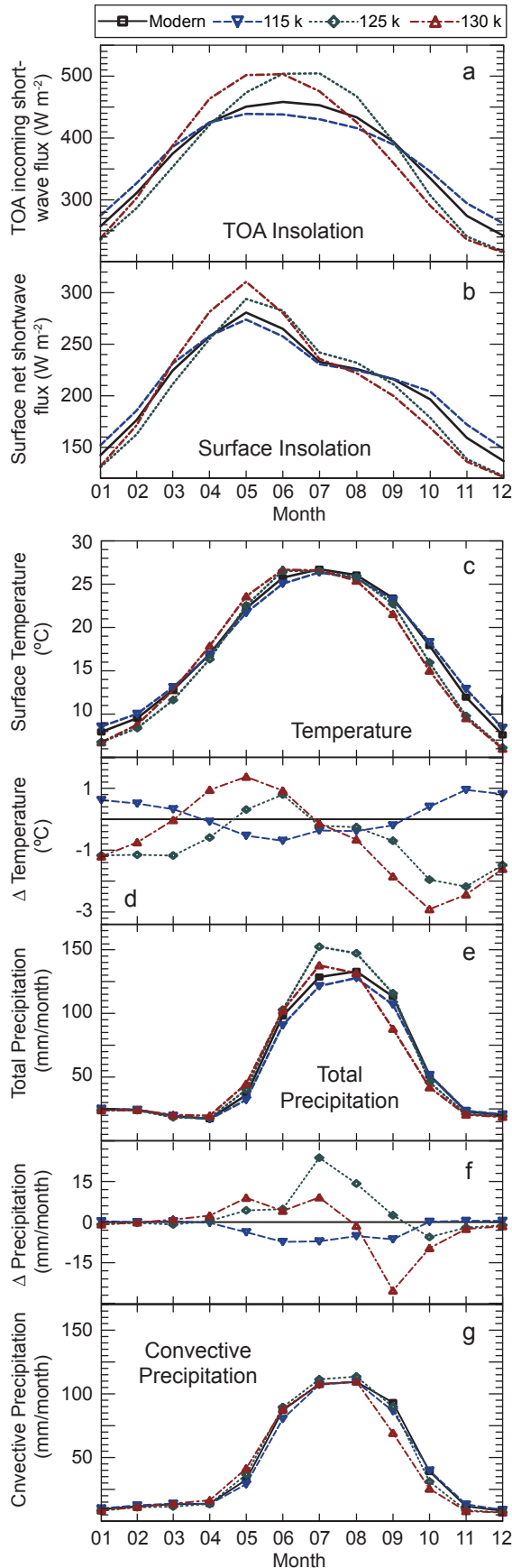


Figure 2: Simulated forcing factors and climatic indices averaged over the North American Monsoon region for 4 cases: modern (black line), 115 ka (blue line), 125ka (green line), and 130 ka (red line). (a) Incoming solar radiation at the top of the atmosphere indicates higher incoming shortwave flux during the early LIG. (b) Surface net shortwave flux highlights cloud feedbacks during the summer months. (c) and (d) Surface temperature and highlighted differences in temperature between case studies and modern. (e) and (f) Total precipitation and differences in precipitation between case studies and modern. (g) Convective precipitation. Large differences in total precipitation, but small differences in convective precipitation during the Eemian highlights the impact of additional large-scale transport of moisture into the study area.

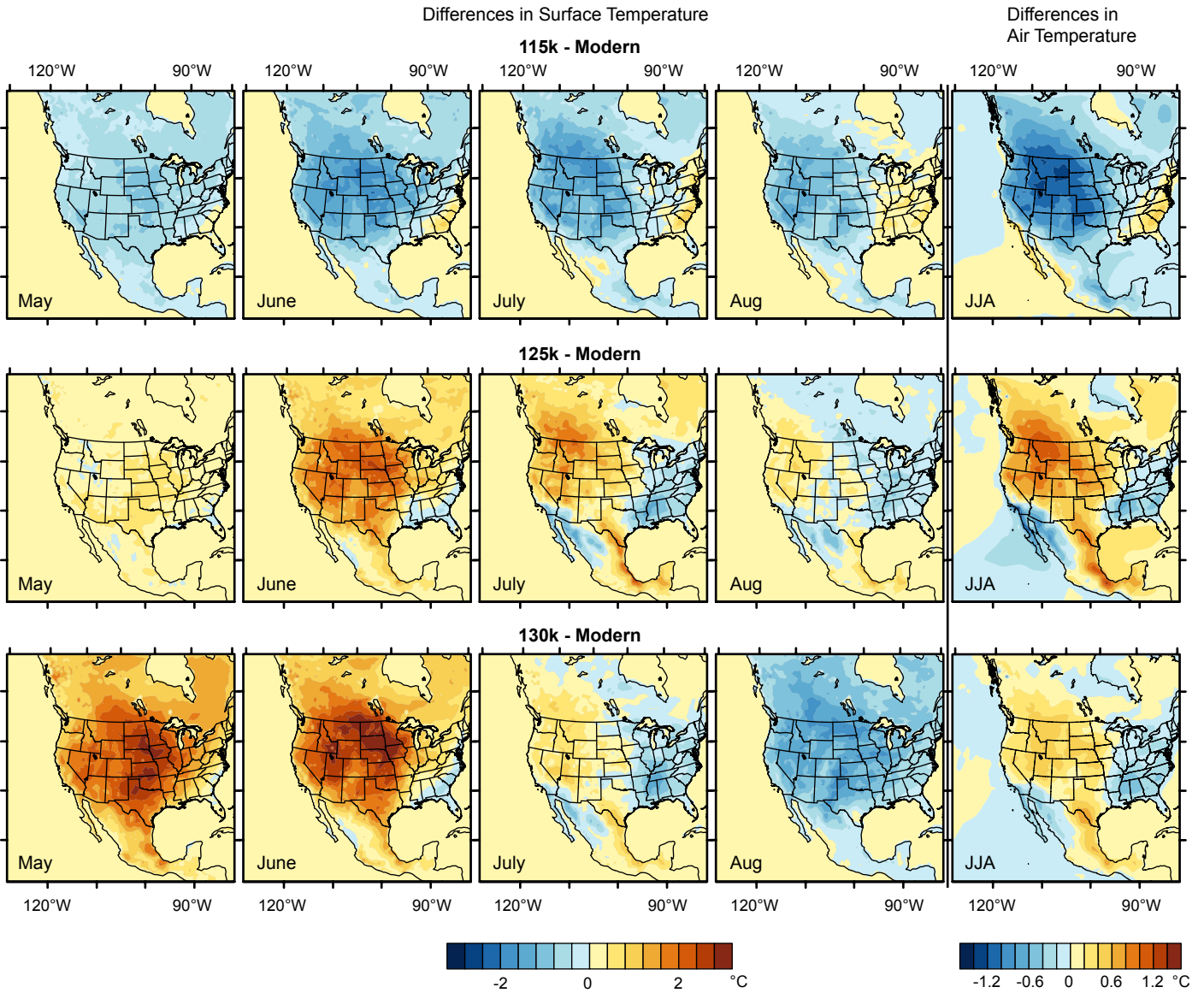


Figure 3: Simulated temperature differences between LIG and modern from May to August. Top row: Difference in temperature between MinObliquity and modern. Middle row: Temperature differences between Eemian and modern. Bottom row: Temperature difference between MaxObliquity and modern. The monthly maps indicate surface temperature with fixed ocean temperature. Notice lower temperatures in July and August in the NAM region. The right column shows near surface air temperature differences averaged over June, July, August. Air temperature increases over the Gulf of Mexico and decreases over the Gulf of California during the Eemian and 130 ka.

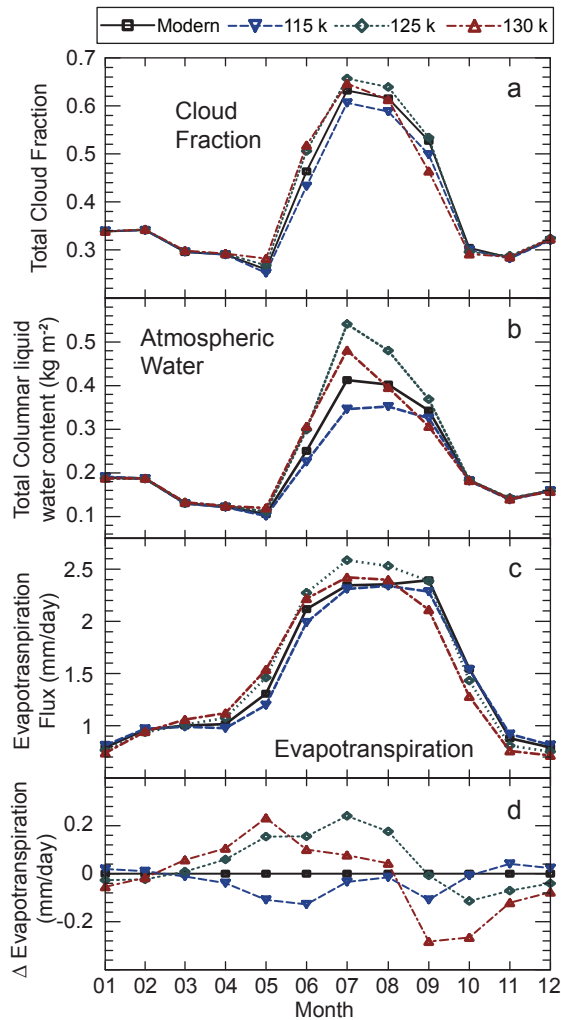


Figure 4: Simulated forcing factors and climate variables averaged over the North American Monsoon region for 4 cases: modern (black line), 115 ka (blue line), 125ka (green line), and 130 ka (red line). (a) Total cloud fraction (b) Total liquid water content. (c) and (d) Total evapotranspiration flux and difference in evapotranspiration between case studies and modern. All graphs indicate an increase in atmospheric moisture during the early LIG.

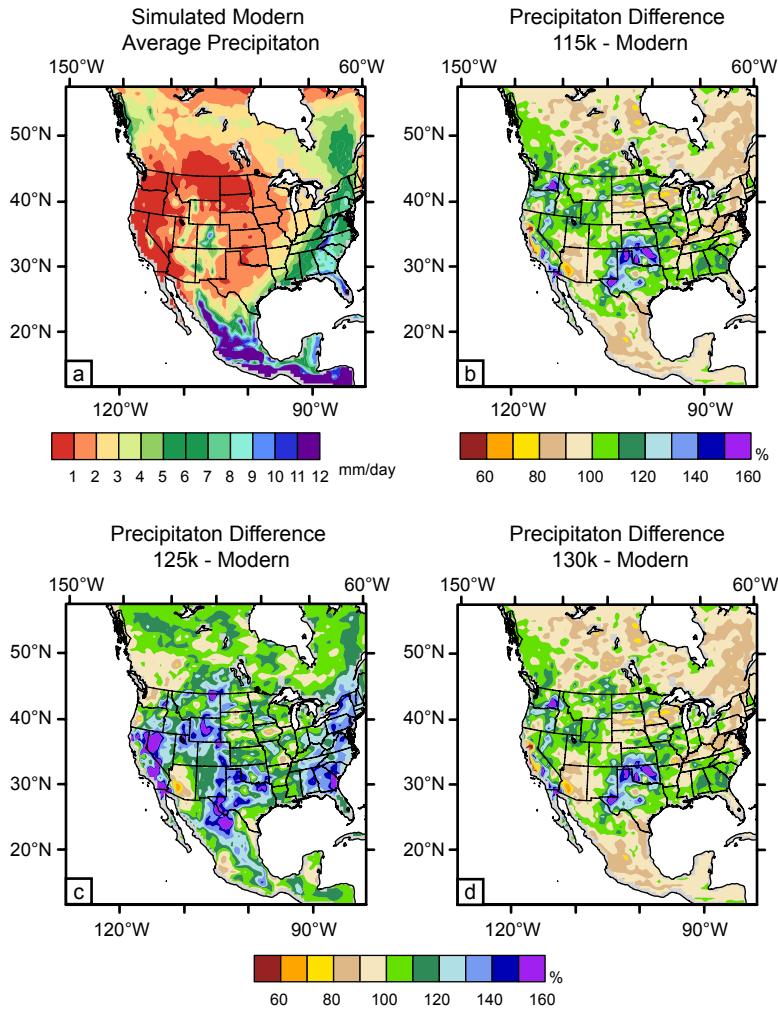


Figure 5: Simulated precipitation differences (in percentage) between LIG and modern for July, August, September (JAS). (a) Simulated JAS precipitation (in mm/day) over the U.S. (b) Difference in precipitation between MinObliquity and modern; (c) Precipitation differences between Eemian and modern; (d) Precipitation difference between MaxObliquity and modern. Notice strong duality pattern between Arizona and eastern monsoon region during 125 ka.

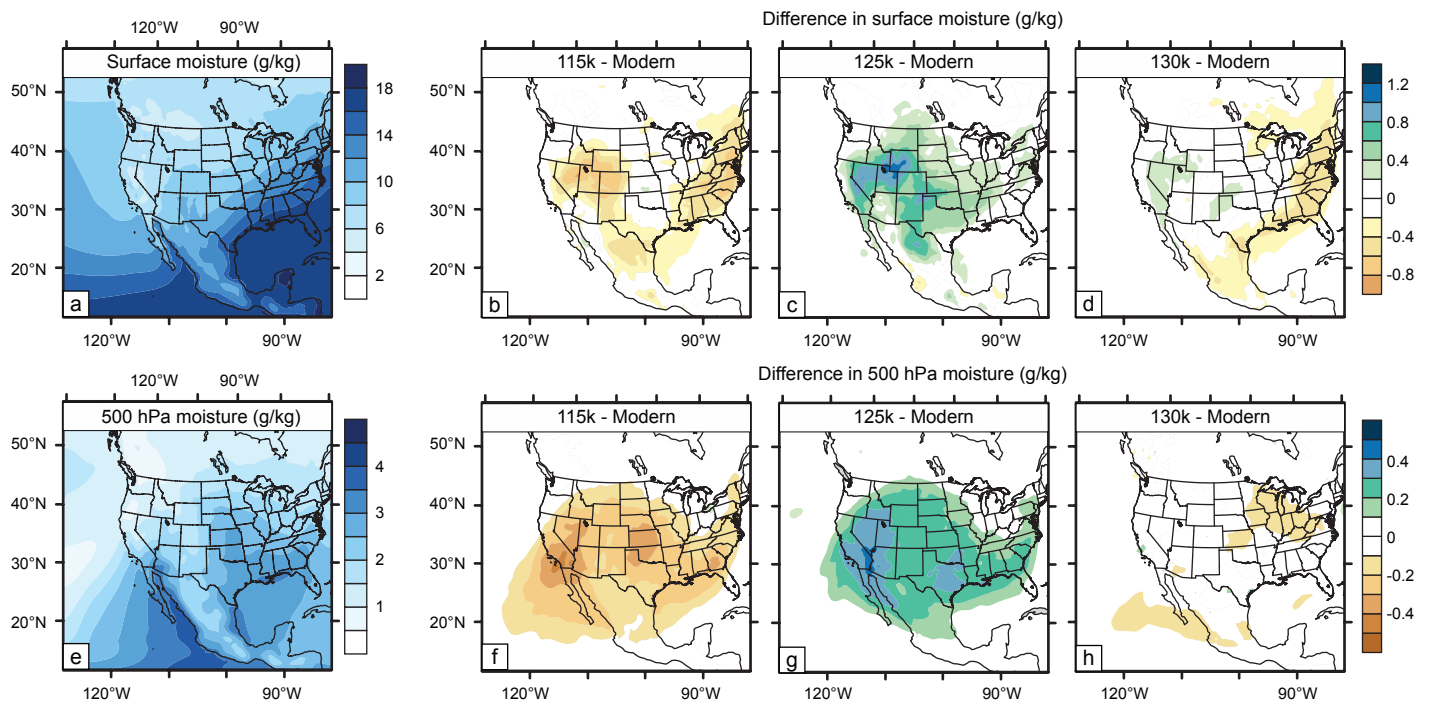


Figure 6: Distribution of specific humidity averaged over July, August, September. (a) Surface moisture; (b-d) Difference in surface specific humidity between LIG case studies and modern; (e) Modern humidity at 500 hPa; (f-h) Humidity difference at 500 hPa between (d) LIG case studies and modern. Notice the increase in humidity at different atmospheric levels during the Eemian.

Simulated modern Wind pattern

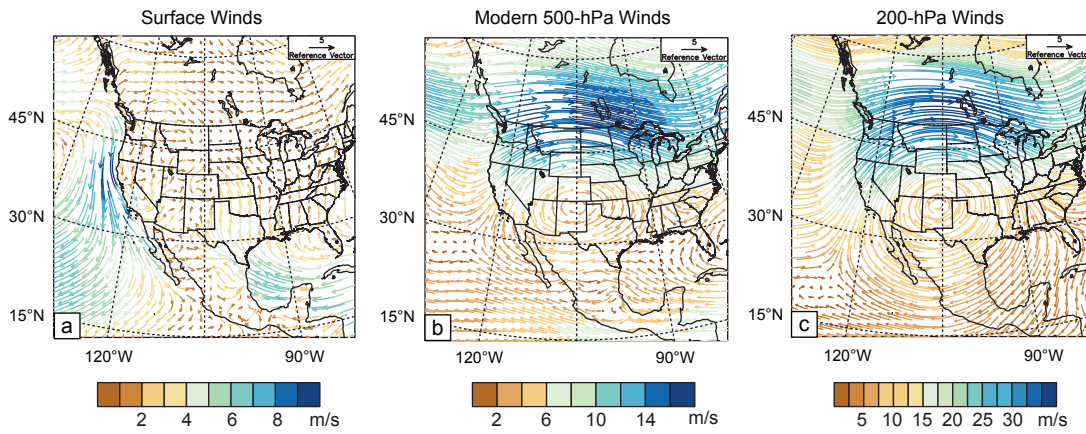


Figure 7: Wind patterns averaged over JAS in the Modern and during the Eemian. (a-c) Modern winds at the surface, 500-hPa, and 200-hPa. The model realistically simulates the anticyclonic patterns at mid- and high-levels. (d-e) Vectors are showing difference in wind magnitude under Eemian and modern conditions. Vector colors indicate magnitude, positive and negative signs are related to the change in physical direction of winds.

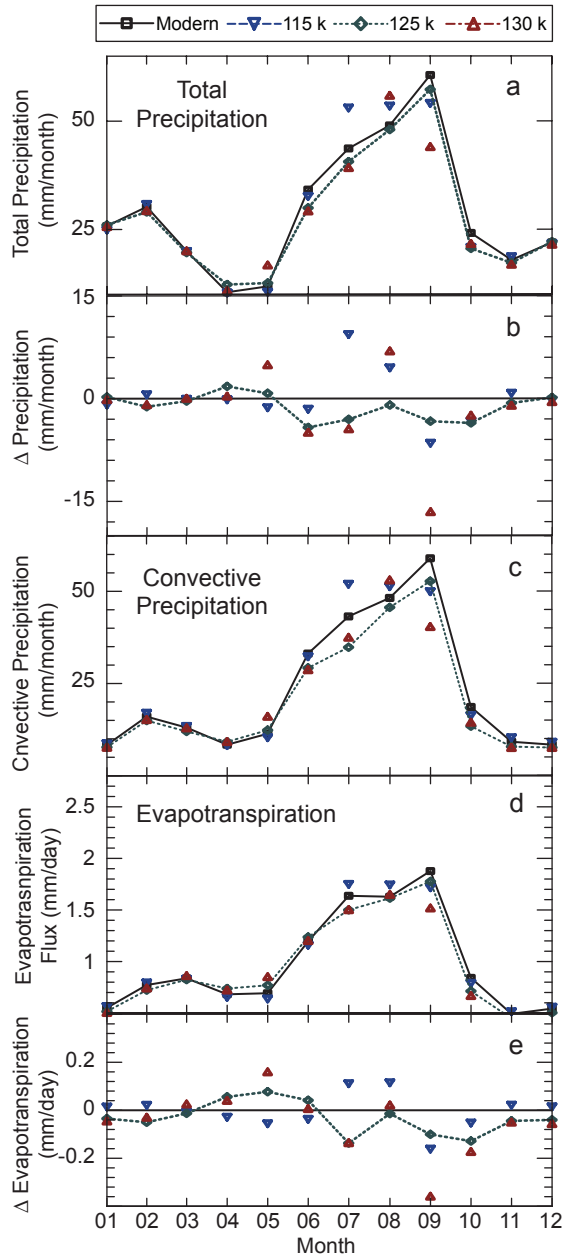


Figure 8: Simulated climate variables averaged over southern Arizona for 4 cases: modern (black line), 115 ka (blue symbols), 125ka (green line), and 130 ka (red symbols). (a-c) Total Precipitation, precipitation difference, and convective precipitation. Precipitation is decreasing during the Eemian summer months across southern Arizona. (d-e) Total evapotranspiration flux and difference in evapotranspiration between case studies and modern.

1
2
3
4
5
6
7
8
9
10
11
12
13
14
15
16
17
18
19
20
21
22
23
24
25
26
27
28
29
30
31
32
33
34
35
36
37
38
39
40
41
42
43
44
45
46
47
48
49
50
51
52
53
54
55
56
57
58
59
60

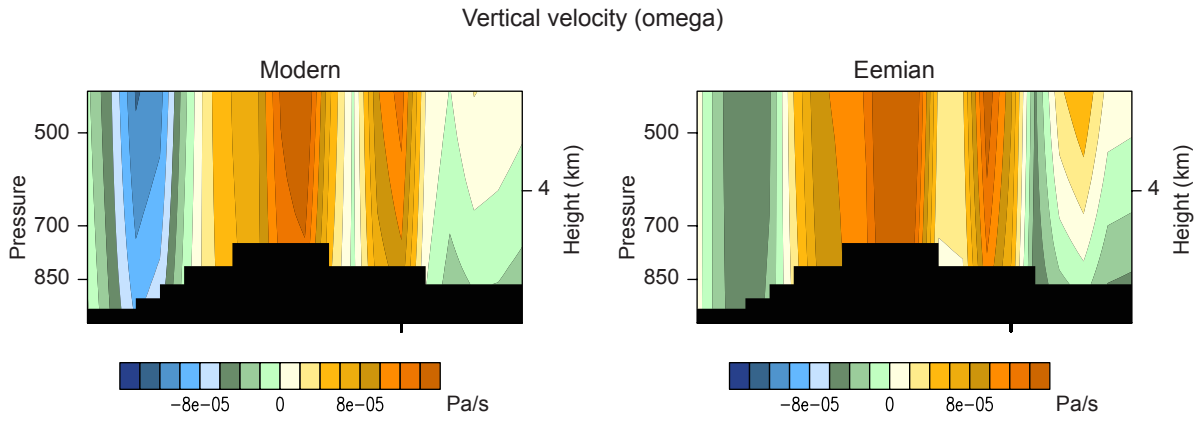


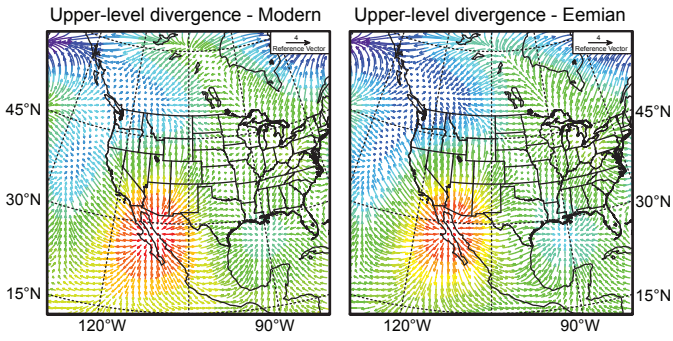
Figure 9: Vertical velocity (ω) across the NAM domain at around 32N during JAS. Height/pressure-longitudinal profile with negative values indicating strong upward air component. (a) Modern simulations. (b) Simulations with Eemian boundary conditions. Notice the reduction in vertical velocity on the western side (southern Arizona).

Table 1: Eemian forcings and boundary conditions:

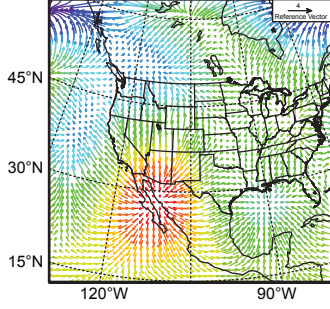
Time*	Orbital Parameters**			Trace Gases		
	ecc	obl	peri	CO2 (ppmv)	CH4 (ppbv)	N2O (ppbv)
0	0.016724	23.446	0.01636	355, 280	760	270
115,000	0.043983	22.438	109.54	273	472	251
125,000	0.042308	23.818	304.76	276	640	263
130,000	0.040129	24.247	225.73	257	512	239

Notes: *Time is in ka; **Orbital parameters are ecc = eccentricity, obl = obliquity, and peri = precession (Berger and Loutre); Trace gases are from <http://www.ncdc.noaa.gov/paleo/icecore.html>

1
2
3
4
5
6
7
8
9
10
11
12
13
14
15
16
17
18
19
20
21
22
23
24
25
26
27
28
29
30
31
32
33
34
35
36
37
38
39
40
41
42
43
44
45
46
47
48
49
50
51
52
53
54
55
56
57
58
59
60



Upper-level divergence - Modern



Upper-level divergence - Eemian

